Spectral reflectance characteristics of the Hamar Laghdad hydrothermal sequence, Morocco: Implications for the methane origin on Mars

Maria Sgavetti[a, *]

maria.sgavetti@unipr.it

Giovanna Serventi[a]

Giuditta Tampella[a]

Giuseppe Pedrazzi[b]

Cristian Carli[c]

Loredana Pompilio[d]

Fulvio Franchi[e]

Claudio Tellini[a]

[a]Department of Physics and Earth Sciences, University of Parma, Parco Area delle Scienze 157/A, 43124 Parma, Italy

[b]Department of Neurosciences, University of Parma, Via Volturno 39, 43125 Parma, Italy

[c]Inaf-IAPS, ~~Tor Vergata,~~ Via Fosso del Cavaliere 100, 00133 Rome, Italy

[d]~~International Research School of Planetary Science,~~Department of Psychologic, Umanistic and Earth Sciences, University of Chieti-Pescara, Via Vestini 31, 66013 Chieti, Italy

[e]CNR-ISMAR, Via Gobetti 101, 40129 Bologna, Italy

*Corresponding author.

Abstract

We analyze and discuss reflectance spectra of carbonate rocks from the Hamar Laghdad area (Morocco), where evidences of interactions with hydrothermal, and, in some cases, methane enriched fluids derived from underlying volcanoclastic rocks, are reported in the literature. Deconvolution of the rock spectra into a sum of Gaussians, using MGM, resolved a number of both vibrational and electronic absorption features, mainly assigned to CO_3^{2-}, Al–OH, and Fe^{2+}, Fe^{3+}, Cu, CF interaction processes, respectively. The associations of these absorption bands are exhaustive descriptions of the rock spectral properties. A spectral model of the Hamar Laghdad carbonate sequence was therefore delineated, based on the integration of these absorption band associations with XRF and Mössbauer analyses of the rock samples. The model involves: pure limestones and dolostones, limestone with iron carbonates, mixed carbonate and Al-silicate impure limestones, limestones with iron sulfides. The model points out the complexity of the spectral characteristics of rocks that underwent hydrothermal and partly methanogenic processes, but also suggests an alternative geologic scenario plausible for possible methanogenic activity in the Mars geologic past.

Keyword: Mars, spectroscopy, geological processes

1 Introduction

Methane emission signature was first observed in the martian atmosphere from orbit (Mcguire, 1977; Formisano et al., 2004), and both orbital and telescopic observations have pointed out methane occurrences as extended plumes localized at distinct latitude and longitude positions, with significant seasonal variation in concentration (e.g., Geminale et al., 2008; Mumma et al., 2009; Fonti and Marzo, 2010). The spatial and time variations are not understandable neither on the basis of the currently known atmospheric parameters, nor by global models of combined atmosphere circulation and chemistry, hence, the mechanisms by which methane is distributed, mixed and lost in the martian atmosphere remain

unknown (Lefèvre and Forget, 2009). Recently, one year of measurements by Tunable Laser Spectrometer (TLS) of the Sample Analysis at Mars (SAM) on Curiosity rover does not report detectable methane concentration in the Gale Crater (Webster et al., 2013), thus supporting the criticism about the existence of active methane sources on Mars.

However, the geologic record of a planet can preserve evidence of possible methanogenic activities in the rock compositions. On Mars, likely sources of methane are inferred to be located in the crust, due to either biotic or abiotic processes, or combined abiotic–biotic transformation processes (e.g., Wallendahl and Treiman, 1999; Formisano et al., 2004; Lyons et al., 2005; Oze and Sharma, 2005; Prieto-Ballestreros et al., 2006; Krasnopolsky, 2006; Atreya et al., 2007), although the geologic contexts in which methane can form are still unknown.

On Earth, the methane abiotic origin overall involves hydrogeological alteration (serpentinization) of ferro-magnesian silicates, implying enriched fluid–rock interaction processes in a wide range of geologic settings. On Mars, a shallow depth, relatively low temperature subpermafrost aquifer is regarded as a feasible environment for methane formation, providing the physical and chemical conditions for reaction of aqueous hydrogen derived from rock alteration by the CO_2 stored in the crust pores (e.g., Wallendahl and Treiman, 1999; Formisano et al., 2004; Lyons et al., 2005; Oze and Sharma, 2005; Krasnopolsky, 2006; Prieto-Ballestreros et al., 2006; Atreya et al., 2007).

The microbial-mediated methane formation was observed in Earth's subsurface environments, where hydrogen-consuming methane-producing microorganisms can be active (e.g., Parkes et al., 1994; Stevens and McKinley, 1995; Gander et al., 2000; Chapelle et al., 2002). The hydrogen, supplying the energy for the methanogenic microbial growth and survival, can either be geochemically produced (Stevens and McKinley, 1995; Chapelle et al., 2002), or derive from hydrogen sulfide species produced by sulfate-reducing bacteria (Parkes et al., 1994; Gander et al., 2000). The result of hydrogen sulfide reaction with various iron species is a range of iron sulfide minerals, that can therefore be found in environments where methanogens thrive (Gander et al., 2000). On Mars, favorable ecological conditions for microbial colonies are, again, inferred to exist in the subpermafrost aquifer environment, where methane can reside in water-saturated fractures and intergranular pores beneath the cryosphere (Boston et al., 1992; Max and Clifford, 2000; Atreya et al., 2007). Both gaseous and in solution methane can be transported to shallower depths from possible deposits at depth in the crust.

Generally, analyses of soil samples and drilling investigations using mass spectrometers, gas chromatographs and laser spectrometers are the only suitable methods to examine the processes of methane formation and destruction mechanisms, responsible for the amount of methane produced and lost. In near-infrared (NIR: 700–1000 nm) and short-wave infrared (SWIR: 1000–2500 nm) reflectance spectra of rocks, alkanes in general have very weak diagnostic absorption features at wavelengths close to the carbonate absorption band positions in minerals (e.g. Cloutis, 1989), thus preventing a reliable discrimination between the two species. Nevertheless, a biologic mediation in methanogenesis causes characteristic micro- and mesoscale textures in the rocks (e.g., Belka, 1998; Cavalazzi et al., 2007; Wendt et al., 2001), and both fully abiotic and abiotic/biotic formation of methane are associated with well defined minerals, involved in fluid–rock interactions as well as acting as catalysts (e.g., Foustoukos and Seyfried, 2004). Mineral assemblages related to methanogenic processes and including sulfide and carbonates (e.g., Parkes et al., 1994; Stevens and McKinley, 1995; Gander et al., 2000), can be recognized by reflectance spectroscopy (e.g., ASTER Spectral Library; RELAB Spectral Database). The potential of this method can be improved by the study of ancient terrestrial analogues, addressed to derive as many as possible of these indirect indicators from accessible areas on the Earth.

In this paper we describe the spectral properties of the rocks outcropping in the Hamar Laghdad area (Morocco) (Fig. 1), where a number of mounds are interpreted to be the result of hydrothermal venting activity in a Devonian sequence of platform carbonate rocks (see a review in Berkowski, 2006). The easternmost mound (Hollard Mound) also provides well documented indication of hydrothermal fluids enriched in thermogenic methane (Peckmann et al., 1999; Berkowski, 2006). We report the results of laboratory reflectance spectroscopy of a set of rock samples, discussing methods of spectra analysis and criteria of band assignments for these complex rock forming mineral assemblages. X-ray diffraction (XRD), X-ray fluorescence (XRF) analyses with particular attention to the identification of minor elements, and Mossbauer spectroscopy were carried out for the interpretation of the electronic absorptions and further refinement of the vibrational band interpretations. The purpose was to set a spectral model of the Hamar Laghdad rocks, based on the reflectance spectral characteristics of mineral assemblages and modifications associated with methanogenesis.

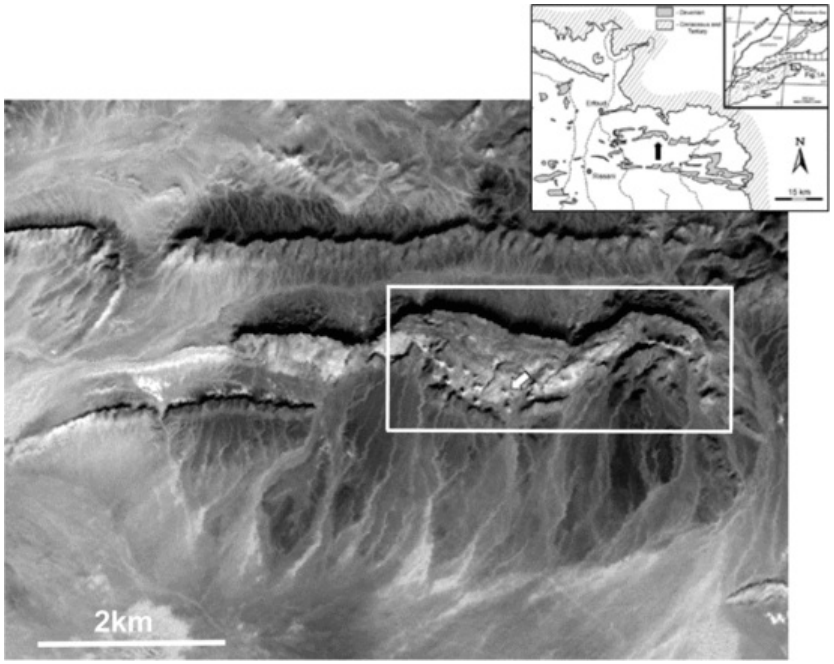

Fig. 1 The Hamar Laghdad area (ASTER image); boxed area: area of provenance of the rock samples analyzed here; white arrow indicates a mound. Inset: the Antiatlas region with location of the Hamar Laghdad (black arrow); gray areas: Devonian units (modified after Belka, 1998).

2 Reflectance spectroscopy of the Hamar Laghdad rocks

Rock samples were collected in the field at the mounds, in intermound areas and in surrounding rock units. Reflectance spectroscopy was made on about 40 samples including limestone, dolostones and volcanoclastites. Fig. 2 shows the set of 15 spectra discussed in this paper, the most representative of the spectral variability of the study area. The spectra were measured on rock slabs using two identical ASD (Analytical Spectral Devices, Inc.) spectrometers, with 350–2500 nm spectral range and 3 nm and 10 nm spectral resolution in the visible–NIR (350–1000 nm) and SWIR (1000–2500 nm), respectively. For one set of samples, the measurements were performed using a High Intensity Contact Probe, with halogen bulb as light source and 10 mm spot size, whereas for a second sample set the configuration was in bi-directional reflectance with 30° incidence–0° emission angles, using a Quartz Tungsten Halogen lamp and ca. 5 mm spot size. In both cases the measurements were made at room temperature and under normal atmospheric pressure conditions. The reflectance spectra are the ratio between the sample ~~row~~raw spectrum and the Spectralon® optical standard corrected for the Spectralon spectral properties. The spectra measured in the two configurations slightly differ in absorption band intensity and width, though the center positions remain unvaried. Consequently, the following spectral analysis is primarily based on band positions, with only qualitative considerations about band intensities for some spectra. The spectra discussed here were measured on clean, smooth and in some cases cut surfaces.

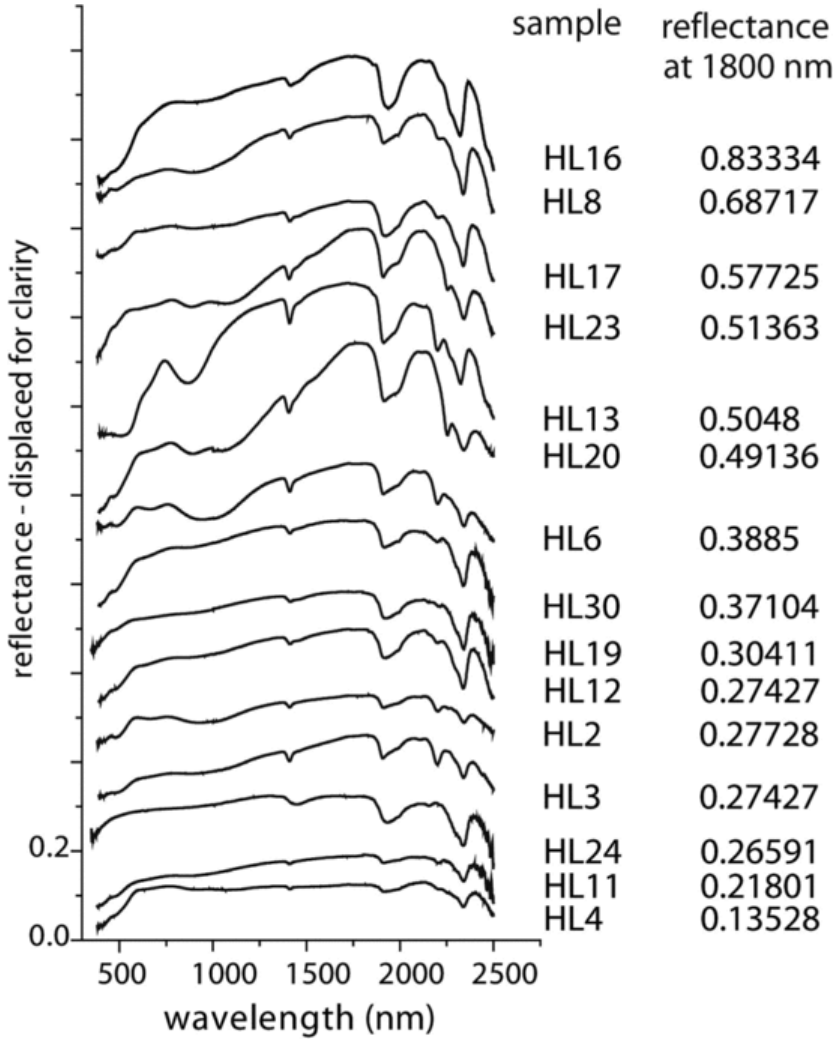

Fig. 2 Reflectance spectra of the Hamar Laghdad samples discussed in this paper; the right hand column reports the reflectance at 1800 nm measured on original, not displaced spectra.

The spectra were analyzed applying the Modified Gaussian Model (MGM) deconvolution routine (Sunshine et al., 1990). MGM was developed and tested for CF electronic absorptions, assuming the average bond length as the variable affecting the energy of the transition. Vibrational absorption bands are generally modeled using Lorentzian functions, with the frequency of a vibration primarily depending on the contributing masses and the forces between them, although a relationship between bond length and energy was empirically observed in vibrational processes (Libowitzky and Beran, 2004). However, deconvolution of vibrational spectra into single Gaussian shaped bands was reported (Gaffey, 1985; Beran et al., 2004), and MGM was already used for the analysis of hydrate mineral spectra (Mustard, 1992). Therefore, MGM was chosen for this study as a convenient tool for comparison with previous vibrational spectra deconvolution. The deconvolution was applied to the whole spectrum, with removal of a continuum tangent to the short wavelength onset of the ~1000 nm band and to the 1700 nm or, in a few cases, 2100 nm peaks. In all the cases presented in this paper, RMS residual error (Sunshine et al., 1990) was between 0.97 and 0.99. Sinusoidal patterns observed in the VIS interval could suggest more complex absorption bands, but adding further components would have increased the correlation between spectral parameters of Intervalence Charge Transfer (IVCT) and Crystal Field (CF) bands. The residuals at both ends of the spectrum are enhanced by relatively low set-up sensibilities in these regions, consequently the absorption features in these intervals are not or only very tentatively considered in the following discussion.

Spectrum deconvolutions of selected samples representative of the principal rock compositions in the Hamar Laghdad area are shown in Figs. 3–5, including different limestone facies, dolostones and volcanoclastites. Tables 1 and 2

show the positions of the Gaussians in the 400–1600 nm and 1700–2600 nm intervals, respectively. The spectral reflectance range of the Hamar Laghdad measurements does not allow the recognition of the prominent 2600 nm absorption band (e.g., Hunt and Salisbury, 1971; Gaffey, 1986), thus this feature is not considered in the following discussion.

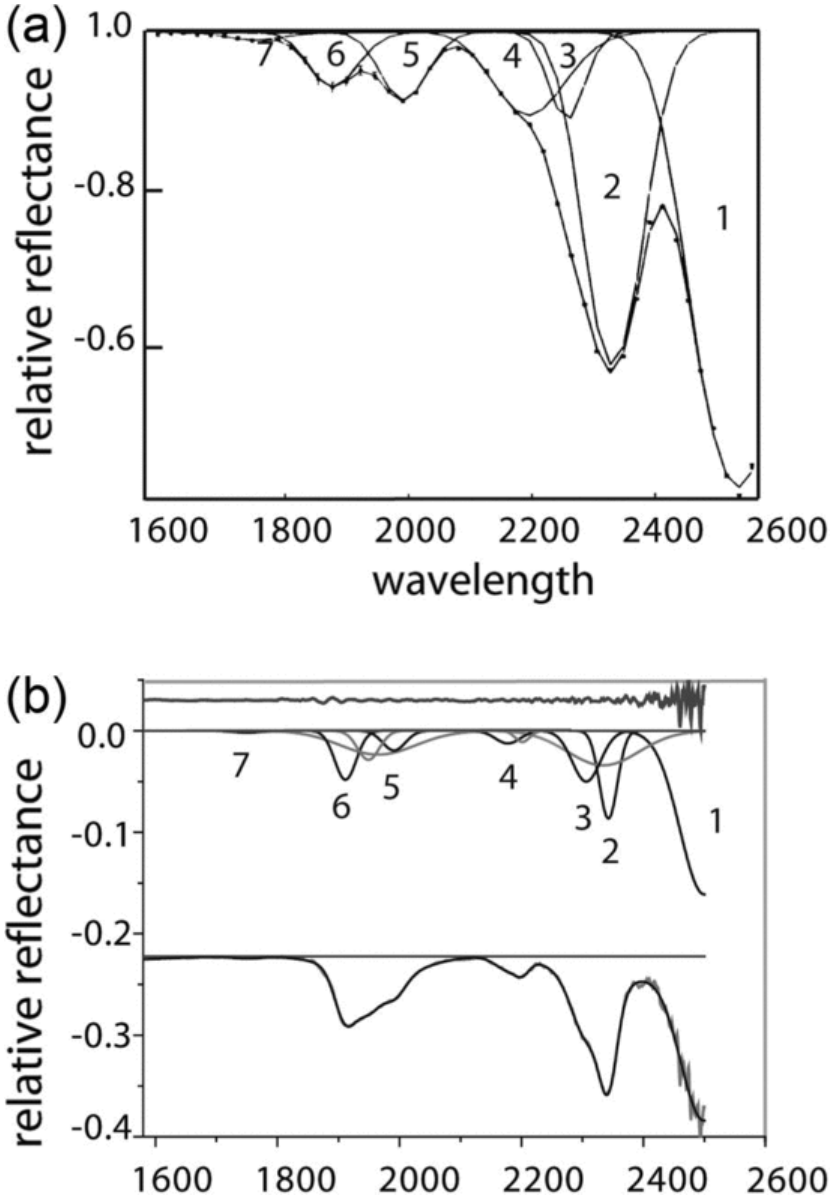

Fig. 3 Recognition of CO_2^{3-} absorption bands in carbonate rock reflectance spectra. (a) Gaffey's (1985) deconvolution of carbonate mineral spectrum; bands 2, 4, 5, 6 assigned to Hunt and Salisbury's (1971) bands II ($3\upsilon_3$), III ($\upsilon_1 + 2\upsilon_3 + \upsilon_4$), IV ($2\upsilon_1 + 2\upsilon_3$) and V ($\upsilon_1 + \upsilon_3$), respectively. Modified after Gaffey (1985). (b) Deconvolution of Hamar Laghdad HL30 rock sample spectrum using MGM (Sunshine et al., 1990). Bottom: continuum removed original spectrum (gray line) fit with Gaussian summation (black line); middle: component Gaussians; top: residuals. Gaffey's (1985) Gaussian numbering used for the carbonate absorptions including the not assigned Gaussian 3 (black lines); Gaussian 6 interferes with a combination mode of water resulting in a bend at longer wavelength than expected (Table 2); see Table 6 for comparison with Gaffey (1985) and Hunt and Salisbury

(1971) band positions; other Gaussians (gray lines) indicate non-carbonate or adjustment bands. In the text, the carbonate bands are indicated as B1–B7.

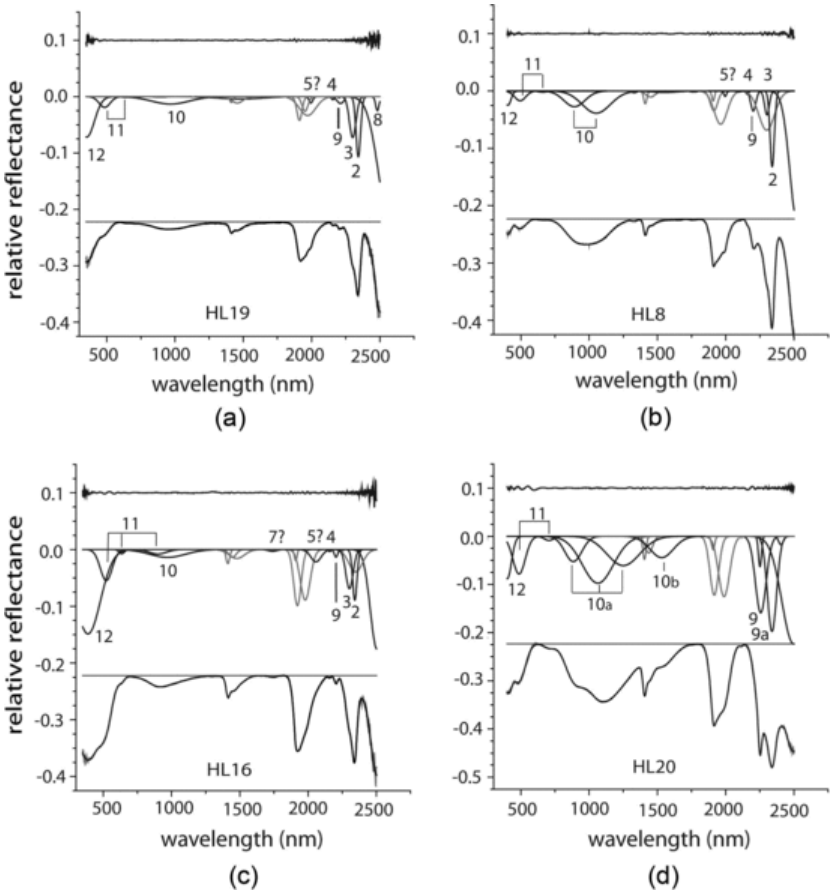

Fig. 4 MGM deconvolution of selected HL rock sample spectra (Table 6). Carbonate bands (2, 4, 5, 7) and Gaussian 3 (black lines) labeled according to Fig. 3b. (a) Limestone (96.3% CaO; 100% calcite); 8: S–O vibrational in sulfates; 9: Al–OH vibrational in hydrates; 10: Fe^{2+} CF in ferrous carbonates; 11: Fe^{3+} CF in ferric oxides; 12: Fe–O OMCT. (b) Limestone (91.23% CaO; 94% calcite, 1% clinochlore, 3.9% muscovite); 10: Fe^{2} CF in ferrous rich carbonate (siderite); 11 and 12 as in (a). (c) Dolostone (57.1 CaO, 36.91 MgO; 2.7% calcite, 96% dolomite, 1.1% aragonite); band assignments as in (a). (d) Volcanoclastite (50.5% SiO_2, 11.82% Al_2O_3; 12.97% MgO, 12.15% Fe_2O_{3tot}; 2.6% quartz, 5.6% dolomite, 60.6% clinochlore, 7.2% low Mg calcite); 9, 9a: vibrational Al–OH and/or Mg–OH; 10a: Fe^{2+} CF in pyroxene and olivine; 10b: Fe^{2+} CF in plagioclase. Other symbols as in (a). See also Tables 3 and 4.

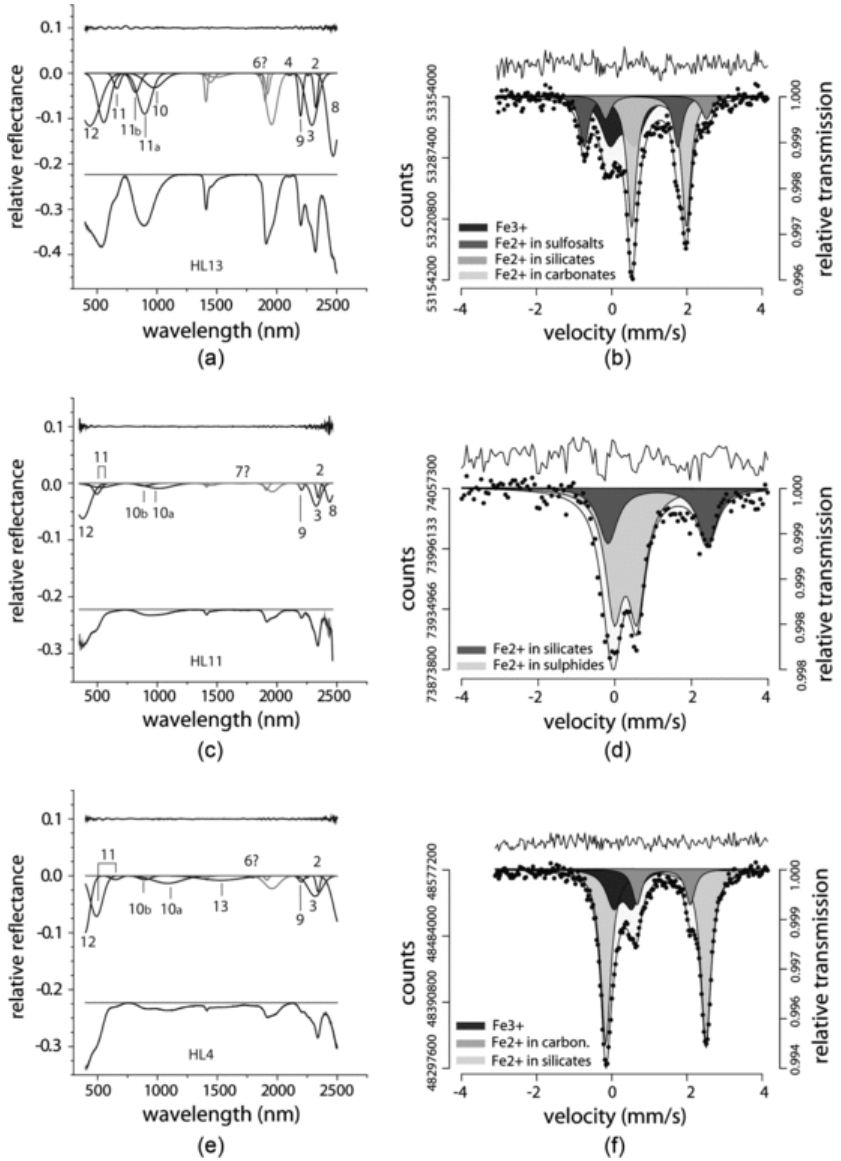

Fig. 5 MGM deconvolution (a, c, and e; Table 6) and relative Mössbauer analysis (b, d, and f) of selected HL sample spectra. Carbonate bands (2, 3, 4, 5, 6, 7) as in Fig. 3b. (a) Dolostone (51.32% CaO, 31.65 MgO; 92.8% dolomite, 3.3% calcite, 4.0% muscovite); 10: Fe^{2+} CF mainly in ferrous carbonates, minor Al-silicate contribution and Cu–Fe sulfosalts; 11a: Fe^{3+} CF in oxides; also possible ferric Al-silicates; 11b: Fe^{3+} CF in oxides and, tentatively, Cu^{2+} carbonates; 11c: Fe^{3+}: CF in oxides. (b) 1: Fe^{2+} in carbonates, 2: Cu–Fe sulfosalts, 3: Fe^{2+} in Al-silicates, 4: Fe^{3+} in paramagnetics. (c) Limestone (87.3% CaO; 95.6% calcite, 0.3% dolomite, 0.5% albite, 0.4% quartz, 2.7% illite, 0.5% clinochlore); 10a, b: doublet (Table 6); Fe^{2+} CF in Al-silicates and ferrous sulfide contribution; high Fe^{2+} concentration in low sulfide modal percent is responsible for the overall reflectance attenuation. (d) 1: predominant Fe^{2+} sulfides, 2: Fe^{2+} in Al-silicates. (e) Limestone (74.7% CaO; 88.6% low Mg calcite, 2.3% dolomite, 2.2% ferroan clinochlore, 2.8% muscovite); 10a, b: doublet (Table 6) due to Fe^{2+} CF in Al-silicates, minor ferrous carbonate contribution to the ~1000 nm band. (f) 1: Fe^{2+} in Al-silicates, 2: Fe^{2+} in carbonates, 3: Fe^{3+} in paramagnetics. Other symbols (8, 9, 11, 12) as in Fig. 4a. See also Tables 3–5, and the text for further explanations.

Table 1 Gaussian center positions in the 400–1600 nm interval: B400–B650 nm: CF in Fe^{3+} oxides and Fe^{2+}–Fe^{3+} IVCT; B820–B1000–B1300 nm: Fe^{2+} and Cu^{2+} in carbonates and silicates, and/or Fe^{3+}, Cu^{+} in silicates and sulfides;

B1410–B1445 nm: O–H; B1500–B1600 nm: Cr in spinel.

Sample	B400 (nm)	B500 (nm)	B650 (nm)	B820 (nm)	B885 (nm)	B950 (nm)	B1000 (nm)	B1100 (nm)	B1300 (nm)	B1410 (nm)	B1445 (nm)	B1500 (nm)	B1600 (nm)
HL2	404	495	678	–	881	–	1003	–	–	1410	1446	–	1562
HL3	401	500	680	–	891	–	–	1064	–	1409	1446	1492	–
HL4	394	491	649	–	894	–	–	1085	–	1411	1447	1529	–
HL6	409	500	677	–	880	–	1027	–	–	1410	1445	1510	–
HL11	379	485	–	–	881	–	996	–	–	1411	1445	–	–
HL17	394	505	645	–	898	–	–	1082	1317	1410	1450	1510	–
HL8	405	495	666	–	892	–	–	1052	1330	1411	1449	1554	–
HL13	438	556	664	822	897	–	977	–	–	1409	1445	1495	–
HL12	422	501	664	–	906	–	–	1092	1260	1411	1453	1536	–
HL23	397	486	690	–	882	–	–	1118	1341	1407	1440	1535	–
HL20	403	484	698	–	884	–	–	1105	1315	1405	1438	1523	–
HL16	388	522	635, 650	–	900	–	971	–	–	1412	1446	1478	1523
HL24	350	499	–	–	873	–	–	1066	–	–	1443	1536	–
HL19	354	485	637, 688	–	891	–	967	–	–	1413	1456	1479	–
HL30	414	496	653	–	892	–	–	1013	–	1410	1450	1501	–

Table 2 Gaussian center positions (nm) in the 1750–2500 nm interval: B1750 nm: possible not assigned C–O band 7; B1820–1850 nm: possible C–O band 6; B1900–1920 nm: H_2O; B1960–2000 nm: C–O band 5; B2100–2150 nm: C–O band 4; B2200 nm: Al–OH band; B2250–2300 nm: not assigned Gaussian 3; B2320–2340 nm: C–O band in calcite and dolomite; B2400 nm: possible S–O in sulfates.

Sample	B1750 (nm)	B1850 (nm)	B1900 (nm)	B1920 (nm)	B1960 (nm)	B2000 (nm)	B2100 (nm)	B2150 (nm)	B2200 (nm)	B2250 (nm)	B2300 (nm)	B2320 (nm)	B2340 (nm)	B2400 (nm)
HL2	1793	–	1906	1918	1979	–	2098	–	2200	2250	2303	–	2342	–
HL3	–	–	1904	1918	1976	–	2105	–	2199	2245	–	2319	2341	2433
HL4	1796	–	1912	–	1956	–	–	–	2201	2250	–	2316	2340	–
HL6	1770	–	1905	1918	1976	–	2101	–	2200	2256	2294	–	2337	–
HL11	1773	–	1911	–	1960	–	–	–	2203	–	–	2324	2341	2487
HL17	–	–	1905	1920	–	1984	2059	–	2202	–	–	2312	2341	–
HL8	1765	–	1908	1914	1963	1996	2095	2158	2202	–	2302	–	2340	–
HL13	–	1854	1907	1922	1957		2108	–	2199	2264	2293	–	2326	2471
HL12	–	–	1907	1923	1972	1995	–	2156	2200	2241	–	2312	2342	–
HL23	–	1896	1906	1925	–	1980	–	–	2220	2252	2289	–	2340	2391
HL20	–	–	1907	1915	–	1985	2115	–	–	2257	–	–	2339	2403
HL16	1740	–	1909	1922	–	1979	2058	2158	2204	2250	2303	–	2342	–

HL24	1739	1875	–	1918	1950	1998	–	2155	–	–	–	2315	2344	2497
HL19	–	–	1912	–	1952	1996	–	2156	2201–2208	2252	2301	–	2343	2482
HL30	1750	–	1911	1949	1965	1991	–	2178	2201	–	2306	2334	2343	–

XRF analyses were performed using a CAMECA SX50 (FMP) (Table 3). XRD analyses were made using X'Pert PRO diffractometer with Panalytical High Score Plus program and Rietveld refinement (Rietveld, 1967; Table 4). Information about the oxidation state of iron was obtained by transmission ^{57}Fe Mössbauer spectra on powdered sample (particle size 63–125 μm) at room temperature using a ^{57}Co thin source (Table 5). The spectrometer operated in constant acceleration with a symmetric velocity ranging between ±4 mm/s. The velocity was calibrated against αFe standard. Fitting of spectra has been performed using the software Recoil® (Lagarec and Rancourt, 1998), using doublets of Lorentzian line shape.

Table 3 XRF analysis of selected Hamar Laghdad rock samples.

	Carbonate samples										Mixed carbonate–silicate samples				Non-carb. samples
	HL11	HL4	HL24	HL8	HL13	HL16	HL19	HL30	HL17	HL12	HL23	HL2	HL6	HL3	HL20
% SiO_2	5.94	13.26	3.61	4.19	6.80	2.06	1.73	3.68	5.28	1.88	30.2	48.0	65.0	64.9	50.5
TiO_2	0.18	0.27	0.06	0.13	0.22	0.07	0.06	0.08	0.11	0.04	1.58	0.40	0.09	0.11	2.17
Al_2O_3	3.49	4.81	1.26	1.90	4.49	1.20	1.13	1.58	2.40	0.80	9.14	8.68	5.40	5.37	11.82
Fe_2O_{3tot}	1.06	4.18	1.84	1.80	4.07	1.04	0.50	1.56	1.10	0.60	5.90	4.94	2.27	1.59	12.15
MnO	0.09	0.28	0.07	0.15	0.27	0.76	0.09	0.21	0.15	0.10	0.21	0.39	0.13	0.13	0.09
MgO	1.04	1.50	0.86	0.66	31.65	36.91	0.40	0.42	0.58	0.52	2.85	0.92	0.26	0.20	12.97
CaO	87.3	74.7	92.3	91.23	51.32	57.10	96.3	92.8	89.8	96.0	46.8	34.7	23.8	25.0	9.30
Na_2O	0.07	0.12	0.01	0.01	0.07	0.02	0.01	0.01	0.00	0.01	2.73	0.42	1.50	1.29	0.03
K_2O	0.67	0.74	0.14	0.28	0.87	0.14	0.12	0.18	0.42	0.12	0.17	1.65	0.66	0.78	0.57
P_2O_5	0.07	0.15	0.09	0.07	0.06	0.05	0.05	0.05	0.08	0.04	0.95	0.09	0.05	0.04	0.72
Tot	99.9	100.0	100.2	100.4	99.8	99.4	100.4	100.6	99.9	100.1	100.5	100.1	99.12	99.4	100.3
L.O.I.	41.07	38.05	42.44	42.3	43.21	46.36	43.13	42.3	42.05	42.9	28.14	23.1	16.47	17.28	14.86
FeO	0.57	2.43	0.77	0.49	0.77	0.60	0.42	0.38	0.68	0.52	2.79	1.02	0.68	0.84	7.36
Fe_2O_3	0.43	1.48	0.98	1.26	3.21	0.37	0.03	1.14	0.34	0.02	2.80	3.81	1.51	0.66	3.97
ppm															
S	1615	404	955	999	380	669	334	807	145	262	116	292	554	276	282
Sc	<5	<5	<5	<5	<5	<5	<5	<5	<5	<5	<5	<5	<5	<5	<5
V	102	59	60	43	250	19	24	21	26	11	125	63	7	12	175
Cr	21	82	24	23	219	24	15	8	13	62	156	47	7	8	210
Co	3	7	<3	67	10	5	<3	16	17	3	79	23	49	42	44
Ni	14	63	40	131	42	8	4	9	5	5	164	14	<3	<3	219

Cu	23	32	40	38	116	33	21	30	20	21	39	26	17	10	83
Zn	59	50	85	48	156	47	18	29	25	20	93	58	12	9	128
Ga	<5	<5	<5	<5	<5	<5	<5	<5	<5	<5	9	12	<5	<5	20
Rb	26	32	12	13	31	10	10	13	18	10	9	59	25	29	21
Sr	562	459	852	325	100	112	255	415	367	347	961	177	323	304	112
Y	11	30	17	30	17	11	10	30	16	11	20	19	10	8	22
Zr	37	56	16	27	43	20	17	19	23	13	178	108	44	59	217
Nb	<3	6	<3	6	5	<3	<3	3	<3	<3	47	6	<3	3	58
Ba	2552	149	94	79	159	109	71	260	112	137	254	374	239	216	579
La	19	19	<10	<10	20	17	<10	30	14	<10	41	14	16	<10	23
Ce	41	52	10	179	42	29	18	26	<10	12	65	43	30	32	23
Nd	<10	47	30	50	31	30	35	40	25	27	50	16	19	11	20
Pb	<5	15	<5	91	19	<5	8	<5	7	5	5	7	15	12	35
Th	26	26	24	11	33	33	35	26	22	31	12	7	6	6	8
U	27	<3	14	<3	<3	<3	3	<3	<3	<3	8	<3	<3	<3	<3

Table 4 XRD analysis of selected Hamar Laghdad rock samples.

Minerals	Carbonate samples mineral modal abundance (%)										Mixed carbonate–silicate samples mineral modal abundance (%)				Non-carbonate samples mineral modal abundance (%)
	HL11	HL4	HL24	HL8	HL13	HL16	HL19	HL30	HL17	HL12	HL23	HL2	HL6	HL3	HL20
Quartz	0.4	4.1	2.0	1.1		0.2		2.0	5.0	1.0	15.0	30.0	48.9	49.0	26.6
Calcite	95.6		98.0	94.0	3.3	2.7	100	98.0	95.0	99.0	70.0	60.0	33.5	35.0	
Low-Mg calcite		88.6													7.2
Dolomite	0.3	2.3			92.8	96.0									5.6
Aragonite						1.1									
Albite	0.5										10.0	6.0	12.4	11	
Muscovite		2.8		3.9	4.0							1.0	2.9	2.0	
Illite	2.7														
Clinochore	0.5			1.0									2.2	2.0	60.6
Fe-clinochore		2.2									2.0	2.0			

Table 5 Mössbauer parameters of HL13, HL4 and HL11.

Sample	IS (mm s^{-1})	QS (mm s^{-1})	W/2 (mm s^{-1})	Area (%)	Assignment
HL13	1.17(5)	2.68(9)	0.17(6)	9(3)	Fe^{2+} in Al silicates[a]

	1.25(9)	1.46(2)	0.17(7)	44(3)	Fe^{2+} in carbonates[b]
	0.28(6)	0.65(7)	0.30(9)	30(3)	Fe^{3+}
	0.52(2)	2.49(3)	0.15(3)	17(4)	Fe^{2+} sulfosalts[c]
HL4	1.17(4)	2.66(8)	0.163(6)	68(2)	Fe^{2+} in Al silicates[a]
	1.36(2)	1.41(4)	0.15(3)	13(2)	Fe^{2+} in carbonates[b]
	0.29(3)	0.49(5)	0.24(5)	19(2)	Fe^{3+}
HL11	1.12(9)	2.60(8)	0.30(7)	34(7)	Fe^{2+} in Al silicates[a]
	0.28(4)	0.59(3)	0.23(3)	66(4)	Fe^{2+} in sulfides[d]

IS: Isomer Shift, QS: Quadrupole Splitting, W/2: HWHM (Half Width at Half Maximum), A: percent area relative to each component (site population).

[a] Stevens et al.'s (2005) parameters for Al silicates: IS from 1.03 to 1.21 mm/s; QS from 1.86 to 2.90 mm/s.

[b] Minai et al.'s (1992) and Dyar et al.'s (2006) parameters for iron bearing carbonates: IS from 1.23 to 1.36 mm/s; QS from 1.36 to 1.84 mm/s.

[c] Charnock et al.'s (1989) and Dyar et al.'s (2006) parameters for tetrahedrite of various compositions: IS from 0.52 to 0.64 mm/s; QS from 2.28 to 3.13 mm/s.

[d] Dyar et al.'s (2006) parameters for sulfides (pyrite): IS 0.29 mm/s; QS 0.60 mm/s.

2.1 Vibrational bands of CO_3^{2-} and associated functional groups in the Hamar Laghdad spectra

2.1.1 Spectroscopic characteristics

Almost all the Hamar Laghdad spectra show the CO_3^{2-} absorptions in the SWIR region, consisting of a set of bands produced by vibrational processes. Hunt and Salisbury (1971) calculated C–O overtones and combinations of modes occurring in the 1900–2600 nm interval and described the resulting absorption features for a set of pure carbonate minerals with different compositions. Gaffey (1985) modeled these absorption bands with seven Gaussians (Fig. 3a) in spectra of particulate samples of pure calcites, dolomites and aragonites. Five of these Gaussians (number 1, 2 and 4, 5, 6) could be assigned on the basis of Hunt and Salisbury's (1971) calculations. The complex absorption feature centered at about 2335 nm is characterized by asymmetry affecting the short wavelength wing. Gaffey (1985) modeled this feature with tree Gaussians, two of which (number 2 and 4) were assigned to Hunt and Salisbury's (1971) bands II and III, whereas the Gaussian 3 does not apparently correspond to a well-defined interaction process.

The Hamar Laghdad spectra mostly display absorption band patterns closely reproducing the carbonate bands reported by Gaffey (1985) (Fig. 3b, Table 6). However, all the Hamar Laghdad spectra were measured on rock samples, and are therefore expected to include, in addition to the signature of Ca, Mg carbonates, also spectral features of carbonates bearing other cations and other minerals as silicates and oxides. Consequently, our approach was to resolve a high number of Gaussians and to evaluate their significance on the basis of both the literature and specifically performed compositional analyses of the rock samples.

Table 6 (a) Gaussian centers (G, in nm) resolved in Hamar Laghdad spectra of Figs. 4 and 5; (b) carbonate band centers of the Hamar Laghdad spectrum of Fig. 3b, compared with the carbonate ranges of wavelength variation (nm) determined by Gaffey (1986) and Hunt and Salisbury (~~1975~~1971).

G	(a)							(b)		
	HL19 (nm)	HL8 (nm)	HL16 (nm)	HL20 (nm)	HL13 (nm)	HL11 (nm)	HL4 (nm)	HL30 (nm)	Gaffey (nm)	Hunt and Salisbury (nm)
2	2343	2340	2342		2326	2341	2340	2341	2312–2340	2280–2390
3	2301	2302	2303		2293	2324	2316			
4	2201	2158	2158		2108			2212	2150–2201	2050–2210

5	2156	1996	2058					2001	1971–1998	1960–2050
6					1850		1796	1911	1853–1885	1840–1920
7			1740			1773				
8	2482				2471	2487				
9a				2339						
9	2208	2202	2204	2257	2199	2203	2201			
10	967	1052	971	1315	977	996	1085			
10		892		1105		881	894			
10				884						
11	637	660	900		897	485				
11	485	495	649	698	822	457				
11			522		664					
11					556					
12	354		388		438	377	394			
13			1523				1529			

In the Hamar Laghdad spectra analyzed here, the composite band centered at ~2330–2340 nm is generally modeled by a higher number of Gaussians than those resolved in pure mineral spectra (Gaffey, 1985). Our first task was therefore to discriminate between a compositionally significant band 2 and adjustment Gaussians. Fig. 6 shows the relationship between the center positions of MGM Gaussians modeled for this composite feature in the Hamar Laghdad spectra and the Gaffey's (1985) band 2 determined for single minerals. The Hamar Laghdad Gaussians with centers in the 2326–2342 nm range fit the aragonite–calcite band 2 positions of Gaffey (1985). Consequently, the Gaussians with lower wavelength center positions within the composite carbonate feature were considered a description of asymmetry perhaps due to factors somehow related to the rock complex composition.

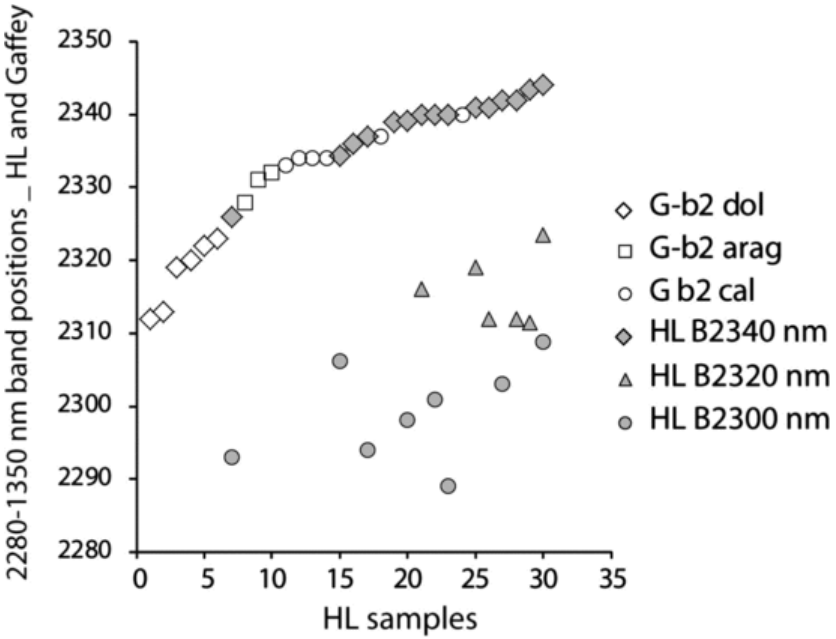

Fig. 6 Center positions of the MGM Gaussians resolved within the about 2330 nm composite band in the Hamar Laghdad sample spectra (HL, gray filled symbols) compared with the positions modeled for single carbonate minerals by Gaffey (1985) (G-b2, black open symbols). The HL Gaussians between 2325 and 2340 nm are considered representative of the carbonate B2 band. Two partly overlapping clusters at shorter wavelengths include Gaussians interpreted as adjustments for the carbonate band asymmetry.

In Fig. 7a, the band center positions of the Hamar Laghdad absorption features between 1700 nm and 2500 nm are plotted vs. the B2 center positions. Positive though highly dispersed variation trends are assigned to carbonate processes (full symbols), consistently with the variation trends for pure minerals (e.g., Hunt and Salisbury, 1971; Gaffey, 1985). In contrast, negative trends (open symbols) characterize the not assigned Gaussians B3 (2250 nm) and B7 (1750 nm). In Fig. 7a, bands B4 and B5 combine the Gaussian center values of bands B2100 and B2150 nm and bands B1960 and B2000 nm, respectively (Table 2), as all occur within the wavelength ranges of Gaffey's (1985) bands 4 and 5 (2150–2201 nm and 1971–1998 nm, respectively) and corresponding Hunt and Salisbury's (1971) bands III and IV (2050–2210 nm, and 1960–2050 nm). In Fig. 7b, the four Hamar Laghdad bands are plotted separately, showing positive relationships with B2 centers for B2150 nm and B2000 nm, thus assumed as more representative of B4 and B5 carbonate bands, whereas B2100 nm and B1960 nm, having negative or almost absent relationships, are considered as adjustment Gaussians.

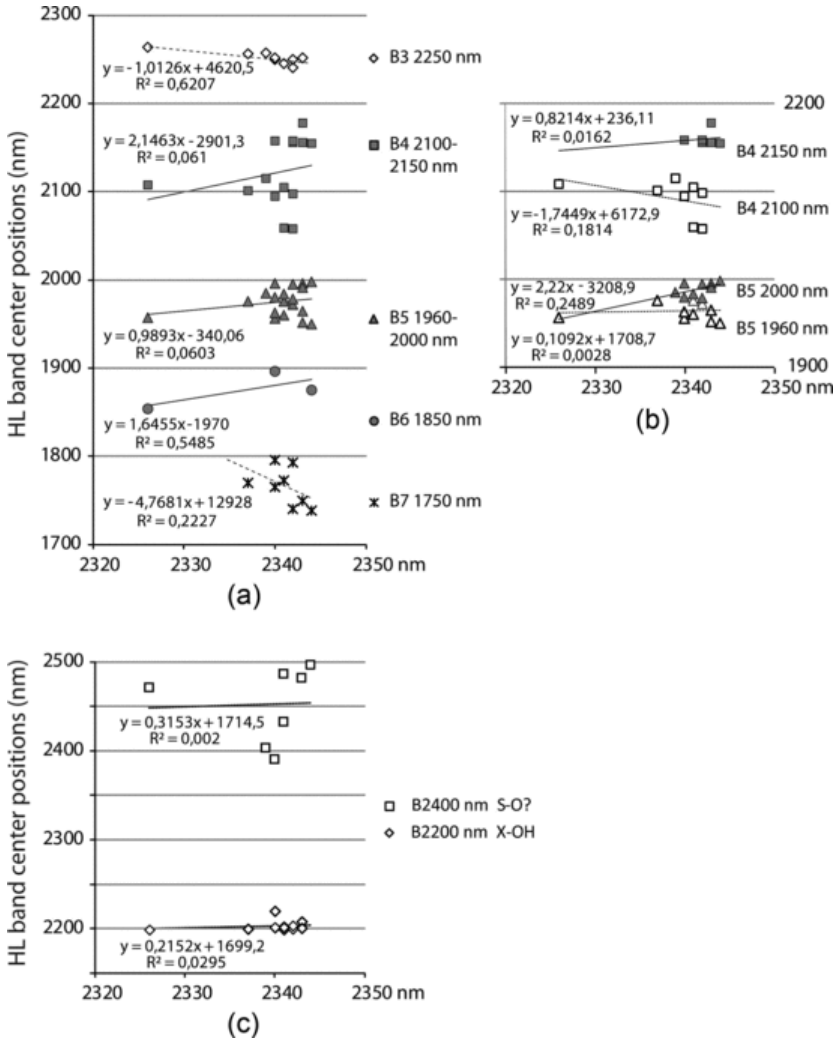

Fig. 7 Variations of Modified Gaussian centers in the 1700–2500 nm interval relative to the B2 Modified Gaussian center variation in the Hamar Laghdad samples (cf. Table 2). (a) Positive variation trends of B4 (combined B2100 and B2150 nm, Table 2), B5 (combined B1960–2000 nm) and B6 (B1850 nm) carbonate bands; negative trends characterize the not-assigned Gaussians B3 and B7; (b) B2150 nm, BB2100 nm, B2000 nm and B 1960 nm are plotted separately: B2150 nm and B2000 nm show positive trends and are assumed as representative of B4 and B5 carbonate bands; the other two Gaussians (B2000 nm, B1960 nm) are considered as adjustment features; (c) almost absent relationships are displayed by non-carbonate bands, assigned to X–OH (B2200 nm) and possibly S–O (B2400 nm) vibrational bands. Linear regression equations and coefficients of determination are reported.

An additional wide Gaussian (not labeled) most often associated with the carbonate band B2 and the Gaussian B3 is considered a further adjustment feature related to the adopted continuum (e.g., Figs. 3b and 4b, c). Other absorptions, showing overall flat variation trends vs. the B2 carbonate band center (Fig. 7c), can be related to interaction processes in other spectroscopic species, as the Al–OH functional group in silicates for the about 2200 nm band (band 9 in Figs. 4 and 5), and the S–O group in sulfate minerals for the about 2500 nm band (band 8 in Figs. 4a and 5a, c; Hunt et al., 1971; Cloutis et al., 2006).

The number of Gaussians recognizable in the 2000–2400 nm interval in the Hamar Laghdad spectra depends on the purity of the carbonate rock composition, which is related to the about 2340 nm band intensity (e.g., Figs. 4a–c, 5a versus 5c and e). For example, the generally weak C–O band 4 occurs in the 2050–2200 nm interval (Hunt and Salisbury, 1971; Gaffey, 1986) with intensities of a few thousandths relative reflectance (e.g., Figs. 4a–c and 5a) and can be masked by the Al–OH vibrational absorption band at 2200 nm.

Bands 5 and 6 are also generally weak and mostly comprised in a composite absorption band together with the 1900 nm absorption of water (e.g., Figs. 4 and 5). The not assigned band 7 can tentatively be identified as a shallow absorption (e.g., Figs. 4c and 5c; Table 3) within the Gaffey's (1985) band 7 interval (1735–1770 nm).

2.1.2 Compositional significance of the vibrational bands in the Hamar Laghdad spectra

Fig. 8 shows the relationships between different rock chemical components and (CaO + MgO) concentrations, assumed here as indicative of the CO_3^{2-} functional group. The samples with (CaO + MgO) content higher than 75% (Table 3) and calcite + dolomite amount above 90% (Table 4) are considered as carbonate rocks in the set of samples discussed here, in contrast with mixed carbonate–silicate rock samples.

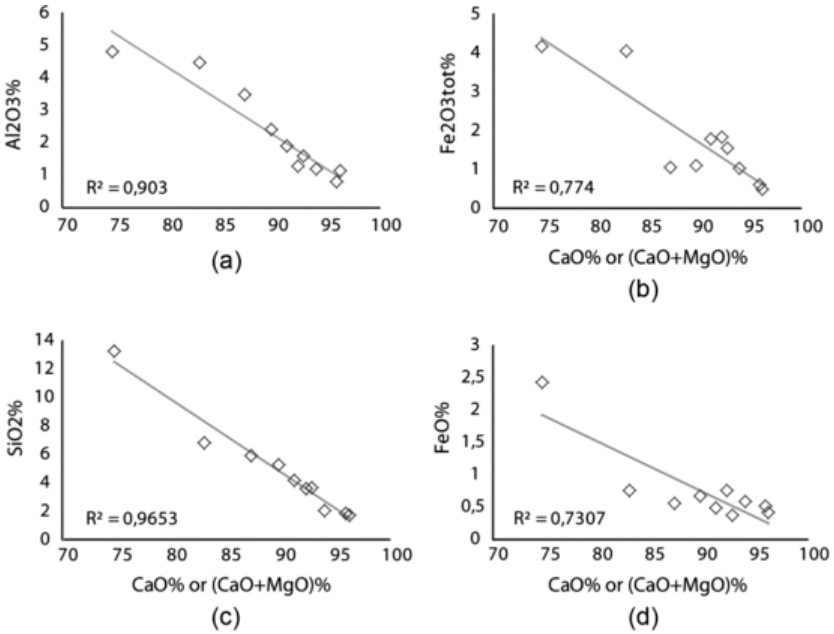

Fig. 8 Variations of (a) Al_2O_3, (b) total iron Fe_2O_3, (c) SiO_2 and (d) FeO concentrations with (CaO + MgO) amount assumed as representative of the CO_3^{2-} functional group in carbonate and carbonate–silicate samples. R^2: coefficient of determination. See also Table 3.

Fig. 6 shows that in about one third of the Hamar Laghdad spectra the position of the B2 carbonate band extends to longer wavelength than the band 2 absorptions in the aragonite–calcite set of spectra reported by Gaffey (1985), although they are within the band II wavelength range (2280–2390 nm) reported by Hunt and Salisbury (1971) for a group of carbonates of different cations. According to the authors, carbonates characterized by long wavelength positions of the $3\nu_3$ overtone band include some calcites, dolomites, siderite, witherite, among others. In the Hamar Laghdad samples, Fe is present with relatively high concentrations both in carbonate and mixed carbonate–silicate samples, and a significant amount of Ba was also observed in some of the carbonate samples, in particular in HL11 (Table 3).

A small number of Hamar Laghdad spectra show the B2 band centers at systematically shorter wavelengths with respect to the other carbonate sample spectra (e.g., Figs. 4c and 5a; Table 1), in agreement with a dolomitic composition supported by XRD results (Table 4) and the high MgO/CaO ratio retrieved by XRF analysis, but also consistent with the presence of Cu carbonates supported by the high Cu concentration in some samples (Table 3; Hunt and Salisbury, 1971; see also the following section for further discussion).

In Fig. 8a and c, the inverse relationships of Al_2O_3 and SiO_2 vs. (CaO + MgO) contents in carbonate samples suggest the possible contribution of Al silicates in some of the spectra consistent with XRD and Mössbauer analyses (Tables 4 and 5).

An additional very weak absorption, though in some cases clearly resolved by a Gaussian, occurs in the 2400–2500 nm wavelength interval (e.g., 8 in Figs. 4a, d, and 5a, c), expressed as a more or less pronounced inflection in the short wavelength wing of the >2500 nm band. This long wavelength band was assigned by Cloutis et al. (2006) to the $3\nu3$ overtone of S–O vibration often in combination with O–H and/or H_2O modes. In all the Hamar Laghdad samples, the XRF results returned variable sulfur concentrations, although in the Hamar Laghdad spectra the end-of-scale wavelength position of the sulfate functional group prevents a fully reliable assignment.

Among the non-carbonate samples, the spectrum of a volcanoclastite (Fig. 4d) is characterized by prominent vibrational bands in the 2200–2400 nm region (9, 9a in the figure), resembling the typical carbonate bands. However, all other carbonate bands are absent and XRF analysis indicated the lowest CaO concentration together with relatively high SiO_2 content in the sample (Table 3), supported by XRD results, reporting small amounts of low Mg calcite and dolomite and high clinochlore content (Table 4). This suggests that the vibrational bands are due to interaction processes in Al and Mg hydroxides (Hunt et al., 1971), involving part of the high Al and Mg concentrations (see the following section for further discussion).

2.2 Electronic absorption bands in the Hamar Laghdad spectra

2.2.1 Spectroscopic characteristics

In the 800–1700 nm interval, the Hamar Laghdad spectra show clearly detectable composite absorption features between 800 and 1300 nm, and in some cases a flattening at about 1500 nm. The MGM routine generally models the about 1000 nm composite absorption with two Gaussians, at about 850–900 nm and between 1000 up to 1200 nm (e.g., Figs. 4b, c and 5). The flattening centered at about 1500–1600 nm is modeled, when detectable, by a very wide and shallow Gaussian.

In the suites of carbonates described by Hunt and Salisbury (1971), Gaffey (1985, 1986) and Gaffey and Reed (1987), a composite absorption at ~800 or 1100 nm is present in all the spectra except for the Sr and Ba carbonate spectra, and is generally attributed by the authors to Fe^{2+}, Fe^{3+} and Cu^{2+} CF electronic transitions. In particular, one band at about 800 nm was observed due to Cu^{2+} in malachite and azurite, and to Fe^{3+} in dolomite samples, whereas composite absorptions at about 1100 nm were detected in magnesite, rhodochrosite, siderite and in general in Fe^{2+} bearing calcite and dolomites.

However, absorption bands due to CF transitions at about 1000–1200 and 800–900 nm are reported in spectra of minerals (e.g., Burns, 1993) that can be found in assemblages related to hydrothermal processes (e.g., Deer et al., 1992). In particular, Fe^{2+} CF transitions in divalent iron bearing Al-silicates, including some alkali amphiboles and micas, produce spectral bands at about 750 or 850 nm always associated with 1000–1200 nm absorptions. The spectra of Fe^{3+} bearing Al-silicates, oxides and sulfates are characterized by Fe^{3+} CF ν_1 bands at slightly longer wavelength (850–950 nm) associated with shorter than 700 nm absorptions. In mixed valence silicate spectra, the ~1000 nm band is often associated with $Fe^{2+} \rightarrow Fe^{3+}$ IVCT in the 600–900 nm interval, e.g., in biotite (IVCT: 733 nm; Fe^{2+} CF: 840 and 1124 nm) and chlorite (IVCT: 699 nm; Fe^{2+} CF: 869 and 1050 nm). Also, particularly intense IVCTs in magnetite produce strong absorption throughout the 700–1300 nm spectral interval, resulting in high opacity (Burns, 1993; ASTER Spectral Library). This mineral can be metasomatically introduced in carbonates, often associated with sulfides and, among others, Cu oxides (Deer et al., 1992). Similarly, Fe^{2+} sulfides as pyrite and pyrrhotite show absorption bands at about 1150 nm, whereas Fe^{3+}–Cu^{+} chalcopyrite spectra are characterized by bands at about 900 nm (after ASTER and RELAB libraries). Sulfide spectra have overall low reflectance and positive slope, the last one particularly pronounced in the featureless spectrum of marcasite, a usually fibrous pyrite dimorph. In other non-calcareous minerals, absorption bands in the 1500–1600 nm region have been reported for Cr^{2+} spinel (Burns, 1993; Cloutis et al., 2004). Large part of the non-carbonate minerals belonging to the groups listed above, derive from hydrothermal alteration of primary ferro-magnesian minerals and can occur in calcareous rocks (Deer et al., 1992), and in particular oxides and sulfides can be possible candidate mineral phases to explain the low reflectance of some of the Hamar Laghdad spectra.

2.2.2 Compositional significance of the electronic bands in Hamar Laghdad spectra

As discussed above, the mineral spectral characteristics reported in the literature and hypothetically expected in the Hamar Laghdad geologic context indicate that the spectroscopic analysis of this set of rocks does not allow unambiguous interpretations for the electronic features. Therefore, we used XRF (Table 3), XRD (Table 4) and Mössbauer spectroscopy (Table 5) of the rock samples to constrain the mineralogical significance of the Gaussians resolved by MGM in the electronic spectral interval.

The spectra in Fig. 5, though belonging to the set of carbonate rocks having calcite + dolomite content above 90% (Table 4) are characterized by complex associations of electronic bands (Fig. 5a) and incomplete carbonate band patterns (Fig. 5c and e).

In the HL13 spectrum of Fig. 5a, three prominent Gaussians (10, 11a, 11b) are resolved by MGM in the 700–1000 nm interval, where various CF transitions in mainly divalent cations in different mineral phases are reported (Burns, 1993). However, in the Hamar Laghdad samples the carbonate band intensity, higher than 0.1 relative reflectance units, suggests that these processes can be related with carbonate chemistries. In particular, Fe^{2+} carbonates can give the major contribution to the ~1000 nm absorption (10 in the figure), consistently with the relatively high FeO and low SiO_2 concentrations detected by XRF in the sample (Table 3). Mössbauer analysis (Fig. 5b; Table 5) supports this interpretation, recognizing a prominent signature interpreted as due to of iron bearing carbonates (Minai et al., 1992; Dyar et al., 2006), though this phase is probably less than 5% and not resolved by XRD (Table 4). Moreover, XRF also measured the highest Cu amount in the sample, suggesting the possible contribution of Cu^{2+} carbonates to the about 800 nm band (11b in the figure; Hunt and Salisbury, 1971). Other iron bearing phases interpreted on the basis of Mössbauer analysis in this sample are: (1) Fe^{2+} bearing Al-silicates (Dyar et al., 2006; Table 5) that can contribute to the ~1000 nm absorption (Burns, 1993), perhaps represented by muscovite (Table 4); (2) Fe–Cu sulfosalts (including tetrahedrite, Charnock et al.'s, 1989; Dyar et al.'s, 2006 values; Fig. 5b, Table 5) that can be tentatively related to the ~900 nm band (11a in the figure), according to the spectral signature of other Cu–Fe sulfides (after ASTER and RELAB libraries); and (3) Fe^{3+} paramagnetic, including oxides, that can be an additional component in the ~900 nm band. The presence of abundant Fe, Cu and S elements could also explain the exceptionally intense spectral feature at about 2500 nm (8 in the figure), tentatively assigned to S–O vibration by Cloutis et al. (2006), thus suggesting iron and/or copper sulfates, which could also contribute to the electronic 900 nm band (Burns, 1993).

A sub-group of carbonate rocks includes spectra characterized by overall low reflectance and spectral contrast. In Fig. 2, the second bottom spectrum, HL11, is also characterized by slightly positive IR slope. The deconvolution in Fig. 5c shows that the

wide, asymmetric and relatively shallow absorption band centered at about 950 nm is resolved into two nested Gaussians at ~900 and ~1000 nm (10b and 10a, respectively; Table 1). The two electronic features are associated with relatively small intensity of the carbonate band, in spite of the high calcite content (95.6%) and relatively high (CaO + MgO) concentration (88.34%; Table 3), thus suggesting the effect of some darkening factor. Mössbauer parameters (Fig. 5d; Table 5) are tentatively interpreted as the signature of Fe^{2+} in sulfides, strongly predominant over that of Fe^{2+} in aluminum silicates (Garg, 1980; Minai et al., 1992; Stevens et al., 2005; Dyar et al., 2006). This dominant phase is consistent with the relatively high sulfur concentration resulting from XRF (Table 3), though probably below the detection limit of XRD analysis (Table 4). On the other hand, the absence of Fe^{3+} paramagnetic phases in Mössbauer results suggests to assign both Gaussian to Fe^{2+} processes, with a possible contribution of Fe^{2+} silicates to the long wavelength Gaussian (10a in Fig. 5d). XRD results indicate the presence of illite and clinochlore (Table 4), also consistent with the two band positions (Table 1; Burns, 1993). Nevertheless, sulfides are also characterized by intense and broad absorptions extended throughout 600 and 1500 nm (after ASTER and RELAB spectral libraries), and can possibly behave as opaque phase reducing the spectral contrast and causing slightly positive slope (cf., Fig. 2).

The bottom spectrum HL4 in Fig. 2 is characterized by flat to slightly negative slope, and by a composite electronic band consisting of a clear doublet, modeled by MGM with two distinct Gaussians at 900 and 1000 nm (10b and 10a, respectively, in Fig. 5e). In this sample, the high amount of carbonate phases (Table 4) is combined with the relatively low (CaO + MgO) concentration (Table 3), as well as the relatively high SiO_2 content and the highest FeO concentrations (2.43%) among the carbonate samples (Table 3) are associated with clinochlore (2.2%) and muscovite (2.8%) retrieved by XRD (Table 4). The results of Mössbauer analysis (Fig. 5f, Table 5) indicate that Fe^{2+} distributed primarily in aluminum silicates (Stevens et al., 2005) and secondarily in iron carbonates (Minai et al., 1992). This allows the tentative attribution of both absorption bands to Fe^{2+} in Al silicates, with minor contribution of Fe^{2+} carbonates and perhaps muscovite to the ~1000 nm band (10a in Fig. 5e), and with Fe^{3+} paramagnetic phases contributing to the 900 nm absorption (10b in the figure). The wide Gaussian at about 1500 nm (13 in the figure) is tentatively interpreted as due to Cr^{2+} transition in spinel (Burns, 1993; Cloutis et al., 2004) consistent with the not negligible chromium concentration detected by XRF (Table 3), even though, if present, it could be below the XRD detection limit.

To complement the Hamar Laghdad spectroscopic framework, the electronic features of a volcanoclastic rock underlying the carbonate sequence are analyzed (Fig. 4d), as it represents a possible source of the enriched hydrothermal fluids that affected the overlying rocks. In this spectrum, a very prominent composite electronic band is resolved into three Gaussians (10a in the figure), that can be assigned to Fe^{2+} CF transitions in Fe–Mg silicates, with high similarity with iron clinochlore spectrum, (USGS, 2007) supported by XRD results (Table 4) and by the high concentration of SiO_2 and FeO resulting from XRF analysis (Table 3). In addition, the prominent absorption band at about 1500 nm (10b in the figure) is again interpreted to be produced by Cr^{2+} in spinel (Burns, 1993; Cloutis et al., 2004), supported by the relatively high content of this element in the sample (Table 3). In this compositional framework, the vibrational bands described in the previous section can be assigned to Al–Mg–OH modes in clinochlore (Table 4).

2.3 Spectral signature of iron oxides in the Hamar Laghdad samples

Almost all of the Hamar Laghdad spectra, even though measured on apparently fresh surfaces, show the signature of iron oxides, characterized by a strong reflectance fall toward the UV with a sharp break at about 500 nm and a weak absorption band at about 600 nm. However, Fe CF transitions in these minerals probably contribute to the broad composite structure in the 800–1500 nm range, mostly decomposed into two Gaussians (Figs. 4 and 5). In particular, the short wavelength ones, occurring in the 880–900 nm interval, can record the superposition of oxide absorptions on other bands occurring in this region.

Absorption bands at about 650 nm and in the 885–960 nm range are assigned by Burns (1993) to Fe^{3+} CF transitions in oxides and hydroxides such as hematite, maghemite, goethite, jarosite and lepidocrocite. In these phases, absorptions interpreted as Fe Oxygen Metal Charge Transfer band in the UV are related with the strong reflectance drop toward the UV.

Hematite is the final product of the alteration of the divalent iron contained in the rocks, and can also be associated with hydrothermal processes. The presence of the ferric oxide signature even in spectra measured on freshly cut sample surfaces, supported by the not negligible Fe^{3+} concentration measured in all samples (Table 3), suggests alteration processes in the bulk of the rocks, thus providing evidence of rock interaction with enriched and possibly subaqueous hydrothermal vents (e.g., Belka, 1998; Mounji et al., 1998).

3 Spectral model for the Hamar Laghdad rocks

The spectra of Figs. 4 and 5 are representative of the overall rock spectral variability in the Hamar Laghdad carbonate sequence. The absorption band associations recognized in the spectra fully describe the rock spectral properties, and allowed us to delineate a spectral model of the Hamar Laghdad hydrothermal system, as defined by previous studies.

According to these studies, fluids enriched by interaction with underlying volcanoclastic rocks seeped through a biogenic carbonate shelf (e.g., Belka, 1998; Cavalazzi et al., 2007; Wendt et al., 2001), modifying the pre-existing carbonate petrographic characteristics. Our XRD, XRF and Mössbauer analyses indirectly recorded this interaction in mineral assemblages in the rocks, including iron carbonates, Al–Mg–Fe silicates and Fe sulfides. These minerals can be interpreted as indicative of hydrothermal processes in neutral and alkaline conditions (e.g., Deer et al., 1992) and have favored, in some cases, possible methane enrichment in fluids (e.g., Chassefière and Leblanc, 2011).

The Hamar Laghdad assemblages we recognized and discussed in the previous sections include: (1) iron and possibly copper carbonates (Table 5), characterized by relatively high Fe^{2+}, Fe^{3+} and Cu concentrations (Table 3) associated with high carbonate mineral abundance (Table 4); (2) mineral assemblages including a non-negligible concentration of some kind of iron–copper sulfosalts (Table 5) and micas (Table 4); (3) iron sulfides (Table 5), consistent with the highest S abundance in some of the samples and associated with relatively high Ba concentration (Table 3), clay minerals and clinochlore (Table 4); (4) Fe^{2+} bearing aluminum silicates (Table 5), including clinochlore which is a product of hydrothermal

alteration of primary Fe–Mg minerals (Table 4); and (5) alteration, deeply affecting the bulk of the rock samples (Fig. 2).

The spectra measured on these rocks are characterized by absorption bands and absorption band associations that can be interpreted on the basis of the mineral phases reported above. Following the same order as above, we observed:

(1) carbonate vibrational bands that occur at longer wavelength positions than expected for dolomites and calcites (Fig. 6), associated with prominent electronic absorption bands in the 700–1300 nm interval (e.g., Figs. 4a–c and 5a, c, e);

(2) clusters of electronic bands resolved by MGM (Fig. 5a) associated with carbonate bands appear to be consistent with Fe^{2+} and Cu^{2+} carbonates (see Mössbauer results in Fig. 5b), contributing to two distinct absorption bands at 1000 and 800 nm, respectively, in which they possibly combine with minor Fe^{2+} silicates and Fe^{3+} bearing phases. The intense absorption at ~900 nm was tentatively interpreted as resulting from the concurrence of Fe–Cu sulfosalts with Fe^{3+} phases;

(3) very low reflectance and spectral contrast of some samples, associated with a shallow composite band in the 800–1000 nm region (e.g., Fig. 5c and d), can result from combined spectral signatures of carbonate and darkening factor; the last one can possibly be represented by iron sulfides recognized by Mössbauer analysis. In this regard, the not negligible Ba concentration leaves open both the question of the contribute of this element to the carbonate signature (e.g., witherite), and the possible effect of almost featureless Ba minerals on the spectral contrast, although these minerals were not detected by XRD;

(4) similar low reflectance and spectral contrast of samples with carbonate composition (e.g., Fig. 5e and f) is associated with a double absorption band in the 800–1100 nm interval that can be assigned to Fe–Al silicates (Table 5); moreover, a well-defined 1500 nm band is observed in some spectra and could be interpreted as due to spinel (Burns, 1993; Cloutis et al., 2004);

(5) the spectral signature of trivalent iron oxides is present in all the spectra (Fig. 2).

Considering the overall spectral shape, the spectra with similar low spectral contrasts (two bottom spectra in Fig. 2) described in points (2 and 3) above are also characterized by: a slightly positive slope (HL11) interpreted as possibly due to the sulfide components and a flat to slightly negative slope (HL4) due to the silicate components in the rock (Pompilio et al., 2007; Carli and Sgavetti, 2011).

4 Implications for Mars

4.1 Carbonate formation and spectroscopic model for Mars

Ca, Mg and Fe carbonates have been recently detected on Mars surface both by Mars Reconnaissance Orbiter's (MRO's) Compact Reconnaissance Imaging Spectrometer (CRISM) (Ehlmann et al., 2008; Michalski and Niles, 2010; Brown et al., 2010) and in situ measurements by instruments on the Spirit Rover (Morris et al., 2010) and Phoenix Lander (Boynton et al., 2009).

From orbit, mainly pure Mg carbonates (Ehlmann et al., 2008) or solid solution of Mg carbonates with calcite and siderite (Brown et al., 2010) were recognized in bedrock in the Nili Fossae, in stratigraphic succession with rocks containing clay minerals, including various Al, Mg, Fe compositions. The geologic context suggested that these mineral assemblages originated via fluid interaction with mafic silicate phases, by analogy with terrestrial hydrothermal processes. Intimately mixed carbonate-high temperature phyllosilicate compositions were observed in rocks exhumed from depth and exposed in the central peak of an impact basin (Michalski and Niles, 2010). The authors favor a metamorphic scenario, in which deep-seated hydrothermal processes alter a mafic protolith in the presence of aqueous CO_2, with subsequent deformation by shock pressure during exhumation. These processes can result in significant methane production (Schulte et al., 2006).

In situ Mössbauer (MB) and Alpha Particle X-ray Spectrometer (APXS) identified Mg–Fe carbonates in the Comanche outcrops within the Gusev Crater, and these observations are consistent with the absorption features due to fundamental vibrational modes of carbonates detected by Miniature Thermal Emission Spectrometer (Mini-TES) in the same outcrops (Morris et al., 2010). Ca-carbonate was identified in Phoenix Landing site by Thermal and Evolved-Gas Analyzer (TEGA) (Boynton et al., 2009). Depending on soil and rock chemistry, either aqueous processes under probable hydrothermal conditions and precipitation of Ca-carbonates from CO_2 supersaturated water (Morris et al., 2010) or, alternatively, volcanic or impact driven hydrothermal alteration (Boynton et al., 2009) were inferred as possible mechanisms for carbonate formation. In synthesis, fluid–rock interaction processes are the most often inferred ways for the formation of carbonates and methane production in different geologic settings on Mars.

On Mars, the spectra detected in the Nili Fossae area showed a wide absorption band in the 1000 nm region and well defined vibrational bands in the SWIR, the latter clearly assignable to the C–O functional group (Ehlmann et al., 2008). C–O band positions occurring at relatively short lambda were assigned to magnesite, whereas the Fe^{2+} 1500 nm absorption was either interpreted as due to the presence of siderite or as a mixture with olivine. The spectrum was therefore interpreted by the authors as indicative of a magnesite–olivine–nontronite mixture, regarded as the result of chemical precipitation from fluids enriched by interaction with rocks and regolith with basaltic composition. Further spectral characterization of the Nili Fossae area recognized clay carbonate alteration assemblages and suggested the presence of iron bearing carbonates instead of magnesium carbonates (Brown et al., 2010).

4.2 Comparison between Mars and Hamar Laghdad spectral models

Beyond the different origins of the Hamar Laghdad and Mars carbonates, both bear evidences of the effects of interaction with volcanic rock related fluids, recorded in rock reflectance spectra. In fact, major similarities between Mars and Hamar Laghdad spectroscopic models relate to the association of vibrational and electronic absorption band patterns, diagnostic of combined carbonate and non-carbonate minerals. For both Mars and Hamar Laghdad, relationships between carbonates and methane are taken

into consideration, at least in the geologic past of the two planets.

However, different geologic scenarios are inferred for Mars and documented for the Hamar Laghdad. On Mars the most compatible interpretation with the planet geologic context is the alteration by hydrothermal fluids of mineral mixtures in a regolith having basaltic composition, a setting that is also inferred consistent with presence of methane in the fluids (Schulte et al., 2006; Ehlmann et al., 2009; Chassefière and Leblanc, 2011). In the Hamar Laghdad, a more complex geologic setting is exposed, for which a direct link between spectral signatures and mineral assemblages associated with hydrothermal processes was established. The spectral model derived from these rocks therefore characterizes a specific geologic system in which methanogenic processes are well documented (e.g., Berkowski, 2006). In particular, the model points out the high spectral diversity produced in rocks that underwent a multi-phase history. Two sequences of processes in fact succeeded: (i) formation of carbonates in an evolving marine shelf environment, and (ii) modification by fluids coming from underlying volcanic rocks which are in turn characterized by a complex spectral signature indicative of circulating fluids.

On Mars, observation of widely diffused carbonates on the surface and of methane in the present atmosphere supported the model of a carbon cycle, both as CO_2 and CH_4, consisting of successive atmosphere–crust interchanges, with carbonates formed by carbon sequestration in the crust and methane released as one of the products of episodic hydrothermal activity involving the carbonates (Chassefière and Leblanc, 2011). The Hamar Laghdad model provides an ancient analogue for this last phase, during which fluids enriched by serpentinization of Fe–Mg minerals printed a signature in the carbonate rocks which still persists after methane dissipation.

5 Summary and concluding remarks

The rock association exposed in the Hamar Laghdad area provided a good data set for a spectroscopic model of carbonate rocks affected by hydrothermal processes. Evidences of complex mixing with hydrothermal and in some cases methane enriched fluids make these rocks a suitable terrestrial analogue for environments in which methane sources can have occurred also on Mars.

Reflectance spectra measured on rock slabs, thus containing the signature of several rock component minerals, represent real natural mineral assemblages, such as those expected in regolith derived from rock disgregation. Spectral deconvolution was able to resolve different components, allowing a reliable assignment of large part of the spectral band associations on the basis of the spectroscopic literature; but in some cases an unambiguous solution required that the spectral patterns were integrated with mineral chemistry data provided by other analytical techniques, including in particular XRF, Mössbauer analyses and XRD.

The resulting spectral model pointed out that the indirect signature of hydrothermal processes and methane vents can also be recorded in subtle absorption features and morphology of the spectral curves. In fact, hydrothermal mineral assemblages include, among others, carbonates with different chemistries and sulfides. Carbonates containing Fe and Cu cations can be recognized in rock reflectance spectra by the association of strong CO_3^{2-} vibrational and Fe^{2+}, Fe^{3+}, Cu^{2+} CF electronic absorptions (e.g., Fig. 5a and b). This spectral signature can be distinguished from that of mixed carbonate-siliceous rock composition, since in the latter spectra the carbonate absorption bands are relatively weak. In these cases of low CO_3^{2-} band intensity associated with Fe^{2+} CF bands, Fe–Al silicates can be inferred (e.g., Fig. 5e, f and Table 5). In addition, in these spectra of mixed composition rocks the low spectral contrast is associated with overall low reflectance and negative spectral slope, typical of most silicate rocks (e.g., HL4 spectrum in Fig. 2).

Recognizing sulfides and sulfosalts in a rock spectrum is a challenging task. Nevertheless, Cu, Fe sulfosalts can contribute to a ~900 nm absorption (e.g., Fig. 5a and b); in contrast Fe^{2+} sulfides strongly absorb in a broad spectral interval centered around ~1200 nm, mostly behaving as opaque phases even if occurring with very low concentrations, with consequent overall reflectance and spectral contrast weakening (e.g., Fig. 5c and d). Moreover, sulfides can produce slightly positive spectral slope, which differentiates this spectral signature from that generally observed in silicate rocks.

This model, grounded on integrated spectroscopic and chemical analyses of terrestrial rocks, can be particularly useful in the interpretation of the new close-range data sets acquired by Curiosity and expected ~~form~~from the different sensors on ExoMars, both providing diagnostic criteria and suggesting cautiousness in the interpretation of in situ spectral reflectance data. Furthermore, it can provide the laboratory data base for the analysis of existing and future data acquired from orbit, to help the exploration of geologic contexts in which hydrothermally and methane modified rocks can have occurred.

However, further work is needed to quantitatively determine the relationship between vibrational carbonate and electronic CF absorption band intensities as a function of carbonate chemistry and rock modal composition, as well as a systematic analysis of the effects of sulfides and other phases behaving as darkening factors.

Acknowledgments

The authors thank IREA-CNR, Milano and IAPS-INAF, Roma for the spectroscopic measurements, the Department of Geosciences, University of Padova for chemical analyses. The authors are also grateful to Jack Mustard and an anonymous reviewer for useful suggestions and comments. Financial support from MIUR and ASI.

References

Atreya S.K., Mahaffy P.R. and Wong A.S., Methane and related trace species on Mars: Origin, loss, implications for life, and habitability, *Planet. Space Sci.* **55**, 2007, 358–369, http://dx.doi.org/10.1016/j.pss.2006.02.005.

Belka Z., Early Devonian Kess-Kess carbonate mud mounds of the eastern Anti-Atlas (Morocco), and their relation to submarine hydrothermal venting, *J. Sediment. Res.* **68**, 1998, 368–377, http://dx.doi.org/10.73-130X/98/068-0368/$03.00.

Beran A., Voll D. and Schneider H., IR spectroscopy as a tool for the characterization of ceramic precursor phases, In: Beran A. and Lebowitzky E., (Eds.), *Spectroscopic Methods in Mineralogy*, 2004, European Mineralogic Union. Eötvös University Press; Budapest, 189–226.

Berkowski B., Vent and mound rugose coral associations from the Middle Devonian of Hamar Laghdad (Anti-Atlas, Morocco), *Geobios* **39**, 2006, 155–170, http://dx.doi.org/10.1016/j.geobios.2004.11.003.

Boston P.J., Ivanov M.-V. and McKay C.P., On the possibility of chemosynthetic ecosystems in subsurface habitats on Mars, *Icarus* **95**, 1992, 300–308.

Boynton W.V., et al., Evidence for calcium carbonate at the Mars Phoenix landing site, *Science* **325**, 2009, 61–64, http://dx.doi.org/10.1126/science.1172768.

Brown A.J., et al., Hydrothermal formation of clay-carbonate alteration assemblages in the Nili Fossae region of Mars, *Earth Planet. Sci. Lett.* **297**, 2010, 174–182, http://dx.doi.org/10.1016/j.epsl.2010.06.018.

Burns R.G., Mineralogical Applications of Crystal Field Theory, 1993, Cambridge University Press.

Carli C. and Sgavetti M., Spectral characteristics of rocks: Effects of composition and texture and implications for the interpretation of planet surface compositions, *Icarus* **211**, 2011, 1034–1048, http://dx.doi.org/10.1016/j.icarus.2010.11.008.

Cavalazzi B., Barbieri R. and Ori G.G., Chemosynthetic microbialites in the Devonian carbonate mounds of Hamar Laghdad (Anti Atlas, Morocco), *Sediment. Geol.* **200**, 2007, 73–88, http://dx.doi.org/10.1016j.sedgeo.2007.03.002.

Chapelle F.H., et al., A hydrogen-based subsurface microbial community dominated by methanogens, *Nature* 2002, 312–314.

Charnock J.M., Garner C.D., Patrick R.A.D. and Vaughan D.J., EXAFS and Mössbauer spectroscopic study of Fe-bearing tetrahedrites, *Mineral. Mag.* **53**, 1989, 193–199.

Chassefière E. and Leblanc F., Methane release and the carbon cycle on Mars, *Planet. Space Sci.* **59**, 2011, 207–217, http://dx.doi.org/10.1016/j.pss.2010.09.004.

Cloutis, E.A., 1989. Spectral reflectance properties of hydrocarbons: remote sensing implications. Science 245, 165--168. DOI: 10.1126/science.245.4914.165.Cloutis E.A., Sunshine J.M. and Morris R.V., Spectral reflectance-compositional properties of spinels and Chromites: Implications for planetary remote sensing and geothermometry, *Meteorit. Planet. Sci.* **39**, 2004, 545–565.

Cloutis E.A., et al., Detection and discrimination of sulfate minerals using reflectance spectroscopy, *Icarus* **184**, 2006, 121–157, http://dx.doi.org/10.1016j.icarus.2006.04.003.

Deer W.A., Howie R.A. and Zussman J., Rock-forming Minerals, second ed., 1992, Pearson Educational Limited; Harlow, England.

Dyar M.D., Agresti D.G., Schaefer M.W., Grant C.A. and Sklute E.C., Mössbauer spectroscopy of Earth and planetary materials, *Annu. Rev. Earth Planet. Sci.* **34**, 2006, 83–125.

Ehlmann B.L., et al., Orbital identification of carbonate-bearing rocks on Mars, *Science* **322**, 2008, 1828–1832, http://dx.doi.org/10.1126/science.1164759.

Ehlmann, B.L., Mustard, J.F-., Murchie, S.L., 2009. Detection of serpentine on Mars by MRO-CRISM and possible relationship with olivine and magnesium carbonates in Nili Fossae. Lunar Planet. Sci. 40, 1787.

Fonti, S., Marzo, G.A., 2010. Mapping the methane on Mars. Astronomy Astrophysics 512, A51. DOI 10.1051/0004-6361/200913178.Formisano V., Atreya S., Encrenaz T., Ignatiev N. and Giuranna M., Detection of methane in the atmosphere of Mars, *Science* **306**, 2004, 1758–1761, http://dx.doi.org/10.1126/science.1101732.

Foustoukos D.I. and Seyfried W.E., Jr., Hydrocarbons in hydrothermal vent fluids: The role of chromium-bearing catalysts, *Science* **304**, 2004, 1002–1005, http://dx.doi.org/10.1126/science.1096033.

Gaffey S.J., Reflectance spectroscopy in the visible and near-infrared (0.35–2.55 μm): Applications in carbonate petrology, *Geology* **13**, 1985, 270–273.

Gaffey S.J., Spectral reflectance of carbonate mineral in the visible and near-infrared (0.35–2.55 microns): Calcite, aragonite, and dolomite, *Am. Miner.* **71**, 1986, 151–162, http://dx.doi.org/0003-004X/86/0102-0151$02.00.

Gaffey S.J. and Reed K.L., Copper in calcite: Detection by visible and near-infrared reflectance, *Econ. Geol.* **82**, 1987, 195–200, http://dx.doi.org/0361-0128/87/643/195-6$2.50.

Gander, W., Parkin, G.-F., Scherer, M.M., 2000. Geomicrobiological interactions among iron sulfide minerals and methanogenic consortia. In: 2000 Conference on Hazardous Waste Research, pp. 78, 79. <http://www.engg.ksu.edu/HSRC/abs44.doc>.

Garg, V.K., 1980. Mössbauer studies of iron sulphide minerals. Revista Brasilera de Fisica, Vol. 10, No. 3.

Geminale A., Formisano V. and Giuranna M., Methane in martian atmosphere: Average spatial, diurnal, and seasonal behavior, *Planet. Space Sci.* **56**, 2008, 1194–1203, http://dx.doi.org/10.1016/j.pss.2008.03.004.

Hunt G.R. and Salisbury J.W., Visible and near-infrared spectra of minerals and rocks: II. Carbonates, *Mod. Geol.* **2**, 1971, 23–30.

Hunt G.R., Salisbury J.W. and Lehhoff C., Visible and near-infrared spectra of minerals and rocks: III. Oxides and hydroxides, *Mod. Geol.* **2**, 1971, 195–205.

Jet Propulsion Laboratory. ASTER Spectral Library – Version 2.0. California Institute of Technology U.S. Government Sponsorship Acknowledged under NAS 620 CL#00-1236. <http://speclib.jpl.nasa.gov/>.

Krasnopolsky V.A., Some problems related to the origin of methane on Mars, *Icarus* **180**, 2006, 359–367, http://dx.doi.org/10.1016/j.icarus.2005.10.015.

Lagarec, K., Rancourt, D.G., 1998. Recoil: Mössbauer Spectral Analysis Software for Windows, Version 1.01998.

Lefèvre F. and Forget F., Observed variations of methane on Mars unexplained by known atmospheric chemistry and physics, *Nature* **460**, 2009, 720–723, http://dx.doi.org/10.1038/nature08228.

Libowitzky, E., Beran, E., 2004. IR spectroscopic characterization of hydrous species in minerals. In: Beran, A., Lebowitzky, E. (Eds.), Spectroscopic Methods in Mineralogy. EMU Notes in Mineralogy, vol. 6, pp. 227–279.

Lyons J.R., Manning C. and Nimmo F., Formation of methane on Mars by fluid–rock interaction in the crust, *Geophys. Res. Lett.* **32**, 2005, L13201, http://dx.doi.org/10.1029/2004GL022161.

Max M.D. and Clifford S.M., The state, potential distribution, and biological implications of methane in the martian crust, *J. Geophys. Res.* **105** (E2), 2000, 4165–4172.

Mcguire W.C., Martian isotopic ratios and upper limits for possible minor constituents as derived from Mariner 9 infrared spectrometer data, *Icarus* **32**, 1977, 85–97, http://dx.doi.org/10.1016/0019-1035(77)90051-3.

Michalski J.R. and Niles P.B., Deep crustal carbonate rocks exposed by meteor impact on Mars, *Nat. Geosci.* **3**, 2010, 751–754.

Minai, Y., Kusudo, I., Matsumoto, R., Sato, H., Tominaga, T., 1992. Moessbauer characterization of sediments from sites 798 and 799, Japan Sea. In: Pisciotto, K.A., Ingle Jr., J.C., von Breymann, M.T., Barron, J., et al. (Eds.), Proceedings of the Ocean Drilling Program, Scientific Results, vol. 127/128, pp. 738–746.

Morris R.V., et al., Identification of carbonate-rich outcrops on Mars by the Spirit Rover, *Science* **329**, 2010, 421–424, http://dx.doi.org/10.1126/science.1189667.

Mounji D., Bourque P.-A. and Savard M.M., Hydrothermal origin of Devonian conical mounds (Kess-Kess) of Hamar Laghdad ridge, Anti-Atlas, Morocco, *Geology* **26**, 1998, 1123–1126.

Mumma M.J., et al., Strong release of methane on Mars in northern summer 2003, *Science* **323**, 2009, 1041–1045, http://dx.doi.org/10.1126/science.1165243.

Mustard J.F., Chemical composition of actinolite from reflectance spectra, *Am. Miner.* **77**, 1992, 345–358.

Oze C. and Sharma M., Have olivine, will gas. Serpentinization and the abiogenic production of methane on Mars, *Geophys. Res. Lett.* **32**, 2005, L10203, http://dx.doi.org/0094-8276/05/2005GL022691.

Parkes R.J., et al., Deep bacterial biosphere in Pacific Ocean sediments, *Nature* **371**, 1994, 410–413.

Peckmann J., Walliser O.H., Riegel W. and Reitner J., Signatures of hydrocarbon venting in a Middle Devonian carbonate mound (Hollard Mound) at the Hamar Laghdad (Antiatlas, Morocco), *Facies* **40**, 1999, 281–296.

Pompilio L., Sgavetti M. and Pedrazzi G., VNIR Reflectance Spectroscopy of pyroxene-bearing rocks: New constraints for understanding planetary surface compositions, *J. Geophys. Res.* **112** (E01004), 2007, 1–23, http://dx.doi.org/10.1029/2006JE002737.

Prieto-Ballestreros O., Kargel J.S., Fairen A.G., Fernandez-Remolar D.C., Dohm J.M. and Amils R., Interglacial clathrate destabilization on Mars: Possible contributing source of the atmospheric methane, *Geology* **34**, 2006, 149–152, http://dx.doi.org/10.1130/G22311.1.

RELAB Spectral Database. Copyright 2008. Brown University, Providence, RI. All Rights Reserved. <http://www.planetary.brown.edu/relabdocs/relab_disclaimer.htm>.

Rietveld H.M., Line profiles of neutron powder-diffraction peaks for structure refinement, *Acta Crystallogr.* **22**, 1967, 151–152.

Schulte M., Blake D., Hoehler T. and McCollom T., Serpentinization and its implications for life on the early Earth and Mars, *Astrobiology* **6**, 2006, 364–376.

Stevens T.O. and McKinley J., Lithoautotrophic microbial ecosystems in deep basal aquifers, *Science* **270**, 1995, 450–454.

Stevens J.G., Khasanov A.M., Miller J.W., Pollak H. and Li Z., (Eds.), *Mössbauer Mineral Handbook,* 2005, Mössbauer Effect Data Center; Asheville, North Carolina, 624pp.

Sunshine J.M., Pieters C.M. and Pratt S.F., Deconvolution of mineral absorption bands: An improved approach, *J. Geophys. Res.* **95**, 1990, 6955–6966, http://dx.doi.org/0148-0227/90/JB-03621$05.00.

USGS Digital Spectral Library, splib06, 2007. <http://speclab.cr.usgs.gov/spectral-lib.html>.

Wallendahl, A., Treiman, A.H., 1999. Geochemical models of low-temperature alteration of martian rocks. Lunar Planet. Sci. XXX, 1268.pdf.

Webster C.R., Mahaffy P.R., Atreya S.K., Flesch G.J., Farley K.A. and the MDL Science Team , Low upper limit to methane abundance on Mars, *Science* 2013, 1–4, http://dx.doi.org/10.1126/science.1242902, <http://www.sciencemag.org/content/early/recent/>.

Wendt J., Kaufmann B. and Belka Z., An exhumed Paleozoic underwater scenery: The Visean mud mounds of the eastern Anti-Atlas (Morocco), *Sediment. Geol.* **145**, 2001, 215–233, PII: S0037-0738(01)00149-X (???).

Highlights

- Lab reflectance spectroscopy of rocks from an ancient (Devonian) hydrothermal system.
- Carbonates affected by hydrothermal and methane enriched fluids from volcanic rocks.
- Integrated spectroscopic, XRF, XRD and Mössbauer analyses.
- Description and assignment of vibrational and electronic absorption bands.
- An analogue to contribute to locate and interpret methane-related processes on Mars.

Queries and Answers

Query: Please confirm that given name(s) and surname(s) have been identified correctly.
Answer: ok

Query: The country name has been inserted for the affiliations. Please check, and correct if necessary.
Answer: ok

Query: Please provide a complete postal address for affiliations.
Answer: ok

Query: Please note that the provided keywords ‘Reflectance spectroscopy and hydrothermal system’ does not match with the list, hence it was removed, so kindly select 3–5 keywords from http://cdn.elsevier.com/promis_misc/yicar_key_words_may2013.pdf. Kindly check and correct, if necessary.
Answer:

ok

Query: References Fonti and Marzo (2010), Cloutis (1989) and Hunt and Salisbury (1975) are cited in the text but not provided in the reference list. Please provide them in the reference list or delete these citations from the text.
Answer: ok

elsevier_YICAR_11270

Query: The citation Wallendahl and Treiman (1992) has been changed to match the author name/date in the reference list. Please check here and in subsequent occurrences, and correct if necessary.

Answer: ok

Query: One or more sponsor names may have been edited to a standard format that enables better searching and identification of your article. Please check and correct if necessary.

Answer: ok

Query: The country names of the Grant Sponsors are provided below. Please check and correct if necessary. ‘MIUR’ - ‘Italy’, ‘ASI’ - ‘Italy’.

Answer: ok